# Effects of quenching rate and viscosity on spinodal decomposition

P. Poesio,* G. Cominardi, and A. M. Lezzi
*Università di Brescia, Via Branze 38, 25123 Brescia, Italy*

R. Mauri
*Università di Pisa, Via Diotisalvi 2, 56126 Pisa, Italy*

G. P. Beretta
*Università di Brescia, Via Branze 38, 25123 Brescia, Italy*
(Received 11 August 2005; published 25 July 2006)

Spinodal decomposition of deeply quenched mixtures is studied experimentally, with particular emphasis on the domain growth rate during the late stage of coarsening. We provide some experimental evidence that at high Péclet number, the process is isotropic and the domain growth is linear in time, even at finite quenching rates. In fact, the quenching rate appears to influence the magnitude of the growth rate, but not its scaling law. In the second part of the work we analyze the effect of viscosity on the growth rate. As predicted by the diffuse interface model, we do not find any effect of viscosity on the growth rate of the nucleating drops, although, as expected, the viscosity of the continuous phase does influence the settling speed and thus the total separation time.

DOI: 10.1103/PhysRevE.74.011507 PACS number(s): 64.75.+g, 05.70.Np

## I. INTRODUCTION

When an initially homogeneous single-phase mixture is cooled across its miscibility curve into the two-phase region, it phase separates either by nucleation or by spinodal decomposition. Nucleation is an activated process with a free energy barrier to overcome, as it occurs when the system is in an initially metastable equilibrium state. Spinodal decomposition, instead, denotes the relaxation to equilibrium of a system that initially is in an unstable equilibrium state, therefore with no energy barrier to overcome. While nucleation is a localized process that proceeds through the formation of nuclei that later grow and coalesce, spinodal decomposition is delocalized, as it occurs simultaneously over the entire domain.

Experimentally, it has been shown that the phase segregation process following a temperature quench can be retarded either by quenching the mixture to a temperature $T$ only by few milli-Kelvin below the critical value $T_{cr}$, namely, to a quench depth $\tau=(T_{cr}-T)/T_{cr}<10^{-5}$ [1–3], or by studying polymer blends with viscosity hundreds times larger than that of water. In these cases, it was observed that, right after the temperature reaches its critical value (corresponding to a point on the miscibility curve), the initially homogeneous mixture starts to separate by diffusion only, leading to the formation of well-defined patches with near-equilibrium concentrations (the local equilibrium hypothesis is currently under debate, as we mention later). The morphology of the mixture under phase segregation depends on the composition of the system: for a critical mixture, the structure is bicontinuous and dendritic-like, whereas off-critical mixtures are characterized by drop-like structures. In the so-called *late stage* of coarsening, single-phase patches grow by diffusion and coalescence, until they become large enough that buoyancy dominates surface tension effects and the mixture separates by gravity. This occurs when the domains have sizes comparable to the capillary length $L_g=\sqrt{\sigma/g\Delta\rho}$, where $\sigma$ is the surface tension, $\Delta\rho$ the density difference between the two phases at equilibrium, and $g$ the gravity field. Typically, for the mixtures used in our experiments, the capillary length $L_g$ is of $O(1\ \mathrm{mm})$. Now, when diffusion is the only active mechanism of growth, it is well known, both experimentally and theoretically [4], that the typical patch size $L$ grows in time as $t^{1/3}$. Therefore, we see that when phase segregation is driven by diffusion, it takes about 1 hour to form millimeter-size domains and subsequently segregate by gravity. This is in fact the case of highly viscous polymer blends, which need such a long time to separate. On the other hand, low-viscosity mixtures separate within seconds from the quench and therefore, in this case, diffusion cannot be the dominant mechanism of phase separation.

The other mechanism of segregation affecting domain growth is convection-driven coalescence, which implies that drops move against each other under the influence of the nonequilibrium capillary force $\mathbf{F}_\phi$. This force and, in general, the convective transport induced by phase transition, is well described by the so-called $H$ model [5], also known as diffuse interface model [6–8], through the minimization of the interfacial energy (see Appendix B). The induced bulk flow predicted by the diffuse interface model has been observed experimentally [9]. The model explains why this effect is much stronger in systems far from equilibrium, i.e., when the composition of the drops and that of the surrounding phase are not equal to their equilibrium values [10]. As shown in Appendix B, the importance of convection relative to diffusion is controlled by the Péclet number defined as the ratio between convective and diffusive mass fluxes $\mathrm{Pe}=VL/D$,

*Electronic address: pietro.poesio@ing.unibs.it

 

where $V$ is the characteristic speed and $L$ a characteristic size of the typical single-phase patches, and $D$ the molecular diffusivity. A reasonable estimate (Appendix B) of the observed velocities for a critical mixture is $V \sim 2\sqrt{2\tau}\chi a/\mu L \sim F_\phi a^2/\mu$, where $\mu$ is the fluid viscosity, $\chi$ is the extra free energy stored within the interface (at equilibrium equal to the surface tension $\sigma$), and $a$ the typical length of the composition inhomogeneities, related to the energy gradient coefficient, as originally defined by van der Waals [11] and to the nonequilibrium capillary force $\mathbf{F}_\phi$ predicted by the model. As a result, the Péclet number can be estimated as $\mathrm{Pe} \sim 2\sqrt{2\tau}\chi a/\mu D \sim 288\tau^6 \rho R T_{cr} D/\mu M_W v_{gr}^2$ where $v_{gr}$ is the growth rate of the domain size $L$. Now, for large Péclet numbers, balancing nonequilibrium and viscous forces, it can be shown that the typical domain size $L$ grows as $t$ [4], which agrees with experimental results, i.e., $v_{gr}$ remains constant during this important phase segregation interval, even while the quench depth $\tau$ increases (in the present experiments by a factor of 4, from 0.006 to 0.026). According to our order of magnitude estimates for the case of a critical mixture, during this linear growth interval, the Péclet number increases as $\tau^6$ (by a factor of 4000 in the present experiments), the surface free energy $\chi$ as $\tau^{7/2}$ and the characteristic length $a$ as $\tau^2$, so that the diffusivity become rapidly overwhelmed by convection.

In addition, simulations based on the diffuse interface model show that $\mathbf{F}_\phi$ is important not only at the onset of phase separation, but during most of the process, as local equilibrium is reached only very late, when the two phases are already fully segregated. Therefore, a full explanation of the segregation mechanisms unfolds by assuming a strong relation between the velocity field and the concentration field, as the thermodynamics of the process is strongly coupled with hydrodynamics. Experimental evidence of the critical role of convection in phase segregation of deeply quenched (1 to 10 K) liquid mixtures is reported in Gupta *et al.* [12], where microdomains are shown to grow linearly in time within the range 10–400 $\mu$m and the coarsening is shown to be almost independent of surface-active compounds, indicating that the driving force is much larger than any surface interactions, which tend to keep the droplets apart.

The separation process of a deeply quenched mixture involves three stages.

*Diffusion stage*. As soon as some inevitable minute disturbances kick a fluid element off the unstable equilibrium state reached upon quenching, the mixture starts to phase separate by diffusion, so that the domain size $L$ grows as $t^{1/3}$. This stage lasts as long as $\mathrm{Pe} \leqslant 1$. When $L$ grows to the same order of $D/V$, convection becomes the dominant mechanism of mass transport.

*Convective stage*. Here growth is dominated by convection-driven coalescence and the domain size $L$ grows as $t$; this stage lasts as long as $L \ll L_g = \sqrt{\sigma/g\Delta\rho}$. When $L$ grows to the same order of the capillary length $L_g$, gravity takes over.

*Gravity driven stage*. After the gravitational crossover, segregation is dominated by the gravity forces induced by the density differences between the two phases.

In this paper, we focus our attention mainly on the convective stage of the process, which determines the total segregation time of the mixture. In particular, our main objective is to investigate experimentally whether (a) quenching rate and (b) viscosity have any influence on the linear growth of single-phase domains which characterizes the convective stage of spinodal decomposition.

The motivation of this research lies in the possible industrial applications [13] of the phase separation process. There, with meter-size devices and deep quenches, the cooling time is comparable to, or even larger than, the characteristic separation time and, therefore, the system starts separating as soon as the coexistence curve is crossed, when cooling is still incomplete. On the other hand, in most of the experiments that have been carried over so far, very shallow quenching or very small systems have been used, where quenching can be considered as effectively instantaneous. At this moment, no experimental data or theoretical calculations are available on how the thermal history may influence the growth of the single-phase domains and the segregation process in general. Accordingly, one aim of this work is to understand, at least qualitatively, what this influence might be, so as to be able to use the cooling rate to control the separation process and check if a slow quenching (slow compared to the characteristic separation time) can induce more than one characteristic length; in that case, the structure factor would be multipeaked, and segregation would be qualitatively different from that experienced in "classical" spinodal decomposition.

In addition, the solvents that are used in industrial applications are often viscous, either because they are naturally viscous or because they become so as a result of chemical reactions (e.g., polymerization) or by adding a modifier (e.g., a surfactant). Accordingly, the other feature that we study in this work, i.e., the influence of viscosity on the phase separation process, is also of obvious industrial relevance.

A brief summary of this work is as follows. In Sec. II we describe the experimental setup and the procedure of the investigation. In Sec. III, we analyze and discuss the experimental results. In particular, in Sec. III A we investigate quantitatively the phase separation of a deeply quenched mixture (both with critical and off-critical composition), while the effects of the quenching rate and viscosity are studied in Sects. III B and III C, respectively. Finally, conclusions are drawn in Sec. IV.

## II. EXPERIMENTAL SETUP

An experimental setup was designed and built to visualize the phase separation process in the size range of 10 $\mu$m to 12 mm. It consists of a thermostatted quartz cell of 1 mm thickness and 8 mm by 45 mm sides. The quartz cell is mounted on one plate of a 6 mm deep water channel (Fig. 1) that provides temperature control. A set of valves switches the water feed between a warm and a cold thermostat, thereby providing the quenching of the sample in the quartz cell. Recording is made by a high-speed, high-resolution, 8-bit digital camera, equipped by macrolenses. Camera resolution is 1024 by 1024 pixels and the frame rate is set either to 75 or 125 fps. The smallest field of view is 1.6

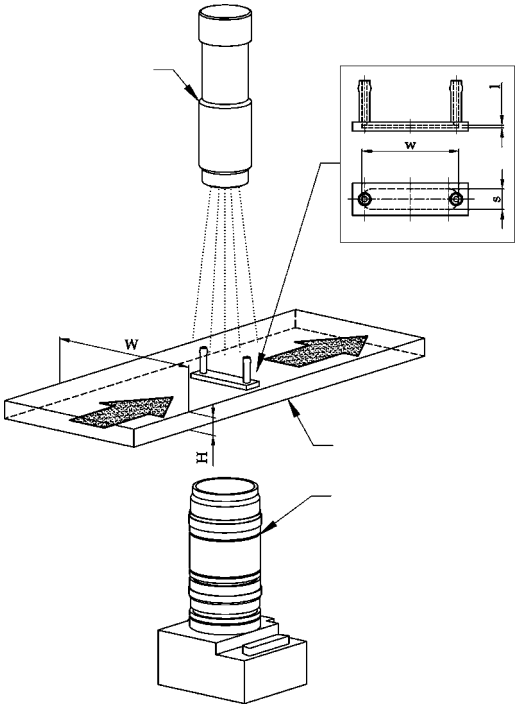


FIG. 1. Sketch of the experimental setup. Arrows indicate the spot light, the quartz cell mounted into the thermostatted support, and the high-speed camera.

by 1.6 mm, with an optical resolution of 5 $\mu$m. The sample is back lighted, using red light to enhance the contrast between phases. The camera is set to an exposure time of 10 $\mu$s and is limited to a focal depth of 5 $\mu$m.

The temperature of the liquid mixture inside the cell is measured by two 0.5 mm *K*-type thermocouples, with response time of 0.05 s. Two thermocouples (1.5 mm diameter) are placed in the cooling channel. All thermocouple acquisitions and the digital camera are triggered with the switching of the water feeding valves that starts the quenching. Measurements are gathered on a PC. Frames, from the videos, are extracted and post-processed with standard and *adhoc* software, written in MATLAB©.

The sample consists of a mixture of water (H2O), acetonitrile (ACN), and toluene (TOL) with critical temperature at 35 °C. Its $\phi$-$T$ phase diagram is reported in Fig. 2 from Ref. [13], where $\phi$ represents the sum of the mole fractions of acetonitrile and toluene. The composition of the mixtures used in this work are reported in Table I, using the thermodynamic data given in Ref. [13]. Mixture $\mathcal{A}$ has critical composition and undergoes phase transition at 35 °C; $\mathcal{B}$ and $\mathcal{C}$ are off-critical mixtures and undergo phase transition at 26 and at 28 °C, respectively. Acetonitrile and toluene are HPLC grade, while water is double-distilled. Crystal violet is added to the solution (50 ppm) to facilitate visualization, as it dissolves preferentially in the organic-rich phase. When dissolved in such small amount crystal violet does not alter the phase diagram. Furthermore, being a cationic emulsifier compound, it makes it ideal to study coalescence during the phase separation of liquid mixtures (see Ref. [12] for more details). Finally, in order to modify the viscosity of the mixture, we add carbossimetilcellulose (CMC, CARBOFIX 5A type) to the solution. CMC is a water-soluble polymer, but it is completely insoluble in the organic phase; we tested that CMC does not act as a modifier (at least up to 10% in weight) and, hence, it does not alter the coexistence curve; up to concentrations of 10%, water-CMC solutions show a Newtonian behavior.

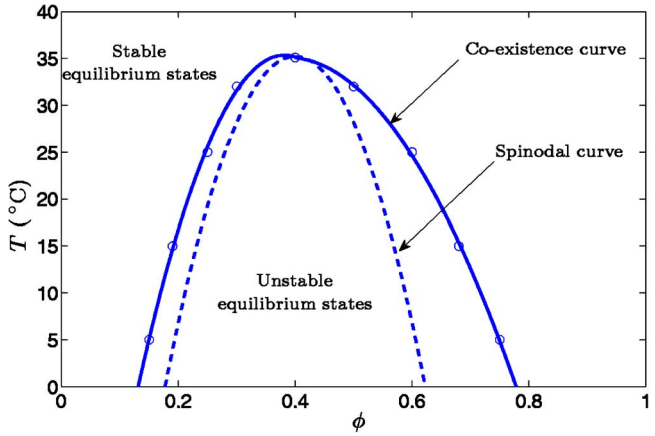


FIG. 2. (Color online) Phase diagram of a water-acetonitrile-toluene mixture where $\phi$ represents the sum of the mole fractions of acetonitrile and toluene. The experimental points are taken from Ref. [13].

In all the experiments, we start with the mixture in its phase separated state, at a constant temperature of 20 °C. The solution is first heated to 38 °C, then mixed thoroughly and, eventually, quenched back below its critical point. Mixing the solution before quenching ensures that the mixture is initially homogeneous. In fact, as shown in Santonicola *et al.* [9], when the system is kept at 38 °C without mixing for two hours, the mixture is still mostly demixed, except for a very thin, few millimeters thick, layer, where a sharp concentration gradient is present.

## III. EXPERIMENTAL RESULTS

### A. Quantitative analysis of deeply quenched mixtures

In this paragraph, we describe the morphology of both critical and off-critical mixtures during phase separation. Figure 3 shows a selection of photograms from a typical sequence obtained for the phase separation of the critical mixture $\mathcal{A}$. As expected, separation occurs simultaneously over the entire field of view, while the mixture exhibits a

TABLE I. Overall compositions (mass fractions) of the mixtures used in the present study. The amount of toluene is kept fixed because of its influence on the coexistence curve. $T_{PT}$ represents the temperature at phase transition.

| Mixture | H2O %w | ACN %w | TOL %w | $T_{PT}$ °C | $M_W$ kg/kmol | $\rho$ kg/m$^3$ |
|---|---|---|---|---|---|---|
| $\mathcal{A}$ | 64 | 35 | 1 | 35 | 22.6 | 912 |
| $\mathcal{B}$ | 77 | 22 | 1 | 26 | 20.7 | 942 |
| $\mathcal{C}$ | 29 | 70 | 1 | 28 | 30.1 | 839 |

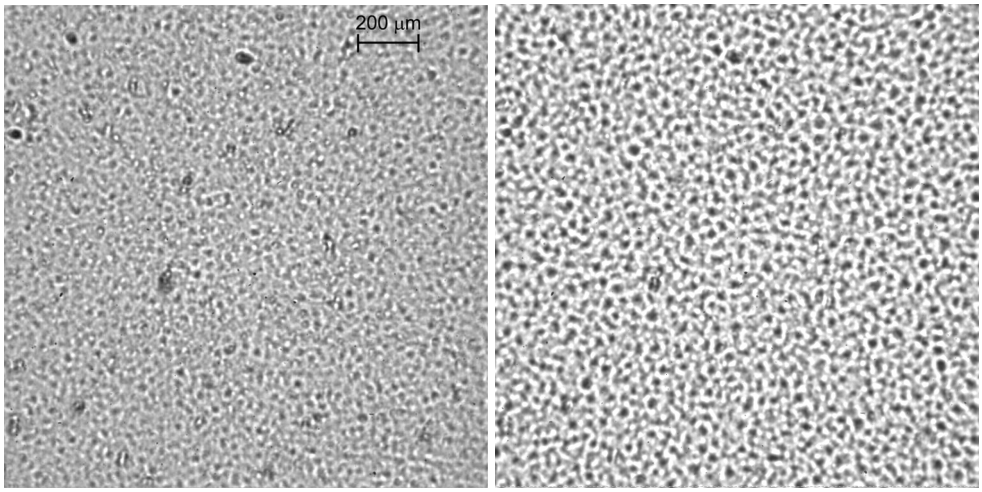


(a) $t = 3.6\ s$; $T = 33.5\,^{\circ}\mathrm{C}$.



(b) $t = 4.0\ s$; $T = 32.5\,^{\circ}\mathrm{C}$.

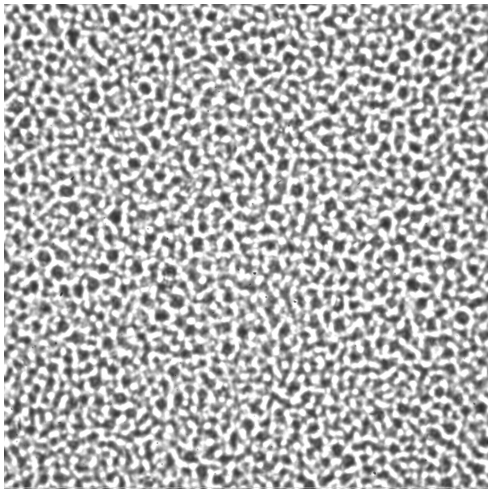

(c) $t = 4.4\ s$; $T = 31.5\,^{\circ}\mathrm{C}$.

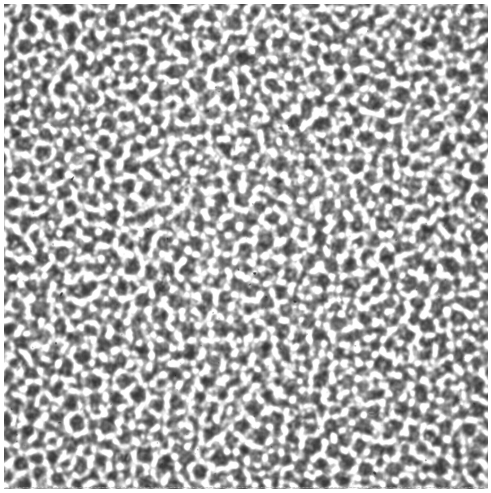

(d) $t = 4.8\ s$; $T = 30.6\,^{\circ}\mathrm{C}$.

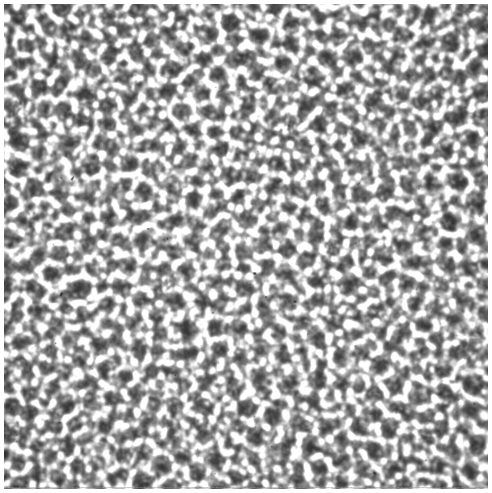

(e) $t = 5.2\ s$; $T = 29.8\,^{\circ}\mathrm{C}$

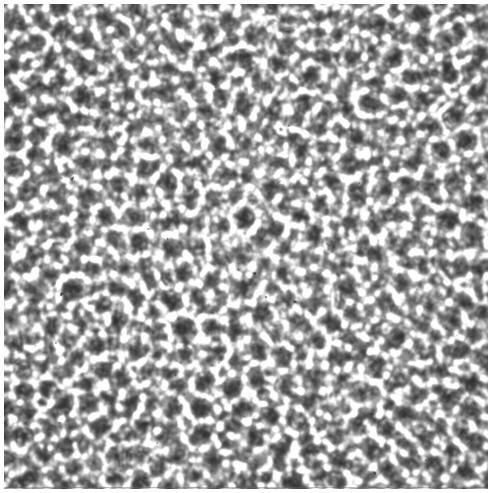

(f) $t = 5.6\ s$; $T = 29.1\,^{\circ}\mathrm{C}$.

FIG. 3. Selected photograms from a sequence of snapshots of decomposition of critical mixture $\mathcal{A}$ (see Table I) showing the typical bicontinuous morphology. Time $t=0$ indicates the instant when the quenching is started. The temperature inside the cell crosses the critical value ($T=T_{cr}$) at $t=3.3$ s. Field of view is $1.6\times1.6$ mm.

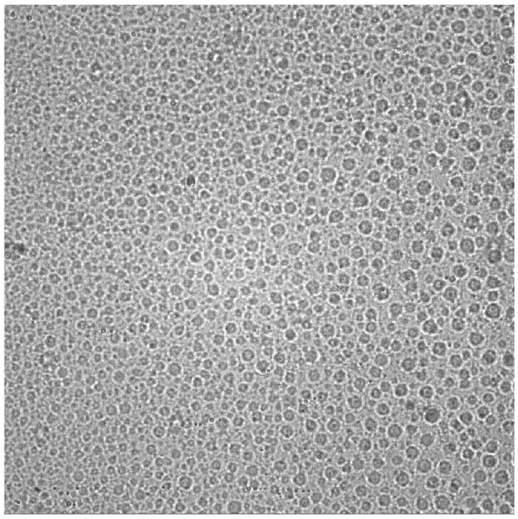

(a) $t = 2.2\ s$; $T = 24.3\,^{\circ}\mathrm{C}$.

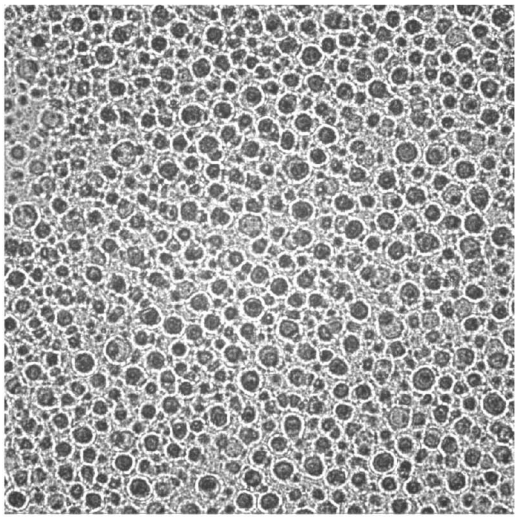

(b) $t = 3.5\ s$; $T = 22.2\,^{\circ}\mathrm{C}$.

FIG. 4. Selected photograms from a sequence of snapshots of decomposition of off-critical mixture $\mathcal{B}$ (see Table I) showing the typical drop-like morphology. Time $t=0$ indicates the instant when the quenching is started. The temperature inside the cell crosses the miscibility curve at $t=1.3$ s.

bicontinuous structure during the entire period. We see that single-phase domains grow very rapidly, as a result of the coalescence induced by their motion, showing that the process is dominated by convection. In fact, when domains reach a typical size $L \approx 35\ \mu$m, we measure speeds $V \approx 1$ mm/s, showing that, since molecular diffusivity is $D \approx 5 \times 10^{-10}$ m$^2$/s, the Péclet number is $\mathrm{Pe} = VL/D \approx 70$. When the gravitational crossover is reached (i.e., $L \approx L_g \approx 1$ mm), the domain size is so large that gravitational effects start playing a role: the motion is not isotropic anymore and the vertical component becomes dominant.

Figure 4 shows a typical sequence for the phase separation of the off-critical mixture $\mathcal{B}$. The structure is now drop-like, with a continuous, water-rich phase and a discrete, organic-rich phase. In this case, too, the process is very rapid and convection driven. Again, after an initial period, gravity takes over and the heavier phase starts sedimenting.

In order to analyze phase separation from a quantitative point of view, we make use of some statistical tools in order to (1) check the isotropy of the process, (2) identify a characteristic length and study its time evolution, (3) analyze the size distribution and the appearance of multiple scales, and (4) spot any violations of the self-similarity hypothesis.

To check the isotropy, we use the method proposed by Wagner [14], who defined the following second order symmetric tensor:

$$d_{xx} = \frac{\sum_{(i,j)} \partial_x^D \phi(x_i,y_j) \partial_x^D \phi(x_i,y_j)}{\sum_{(i,j)} \phi(x_i,y_j)^2},$$

$$d_{yy} = \frac{\sum_{(i,j)} \partial_y^D \phi(x_i,y_j) \partial_y^D \phi(x_i,y_j)}{\sum_{(i,j)} \phi(x_i,y_j)^2},$$

$$d_{xy} = \frac{\sum_{(i,j)} \partial_x^D \phi(x_i,y_j) \partial_y^D \phi(x_i,y_j)}{\sum_{(i,j)} \phi(x_i,y_j)^2} = d_{yx}, \tag{1}$$

where $\partial_x^D \phi$ and $\partial_y^D \phi$ are the symmetric discrete derivatives along the $x$ and $y$ directions, respectively, of the concentration field $\phi(x,y)$ and, in the summation, they are evaluated at each pixel over the entire field of view. The concentration field is derived from the images recorded by the camera and, as done in Gupta *et al.* [12], we assumed that the intensity level recorded by the camera is linearly related to the concentration field. Denoting by $d_1$ and $d_2$ the eigenvalues of the matrix $\mathbf{d}$, with $d_1 \geqslant d_2$, the isotropy of the images can be measured in terms of the isotropy index $\xi = d_2/d_1$, where $\xi=1$ and $\xi=0$ correspond to perfectly isotropic and perfectly anisotropic systems, respectively.

As shown in Fig. 5, for $t>1$ s, we measure $\xi=0.95$, revealing an apparent slight anisotropy during the whole process (at $t<1$ s, phase separation has not started yet). Separate measurements, though, reveal that a perfectly isotropic image (i.e., a circle) also determines a value $\xi=0.95$, so we conclude that this unexpected measurement is due to a defect in the camera CMOS-sensor technology vertical multiplexing. This conclusion is confirmed by the fact that at earlier times, for $t<1$ s, we measure a strong anisotropy, while at that time, since the system is still single-phase, we should be measuring an isotropic background noise. Note that the field of view is very small and it is placed in the bulk of the quartz cell, so that the boundary conditions do not play any relevant role. Wall effects become important when the size of the

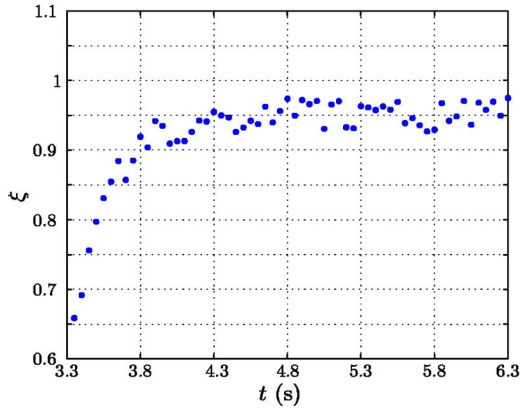


FIG. 5. (Color online) Evolution of the isotropy index $\xi$ (see text) over time for critical mixture $\mathcal{A}$. Ideally, under isotropic condition, this index should be unity. Our measure shows a small deviation from unity; this is due to the CMOS technology of camera sensor. Before the separation begins, $\xi$ shows a very anisotropic condition because the signal-to-noise ratio is very low.

single-phase domains are comparable with the cell thickness (i.e., 500 $\mu$m or larger), but at that point gravity becomes also important.

Next we study the time evolution of single-phase domains by defining a characteristic length of the system. To do that, we do not use $\sqrt{d}$, where $d=d_1=d_2$ is Wagner's lengthscale, because it is very noisy, being based on the pixel-by-pixel derivatives of the concentration field. Instead, we define the characteristic dimension, and its time evolution, in terms of the structure factor $S(\mathbf{k},t)$, indicating the size distribution of the system at time $t$:

$$S(\mathbf{k},t) = \frac{\sum_{\mathbf{k}} \hat{\phi}(\mathbf{k},t)\hat{\phi}(-\mathbf{k},t)}{\sum_{\mathbf{k}} 1}. \tag{2}$$

Here $\hat{\phi}(\mathbf{k},t)$ is the two-dimensional discrete Fourier transform of the concentration field, $\mathbf{k}$ is the wavelength vector, and $k$ its length. First of all, we find that for our data $\hat{\phi}$ is axisymmetric, i.e., $\hat{\phi}(\mathbf{k},t)=\hat{\phi}(k,t)$ confirming the previous observation about the isotropy of the process, so that $S(\mathbf{k},t)=S(k,t)$. In Fig. 6, $\hat{\phi}(\mathbf{k},t)$ is represented at two different times, emphasizing the isotropy of the concentration field.

Defining the $p$-order moment of the structure factor $S(k,t)$ as

$$K_p(t) = \left( \frac{\sum_{k=0}^{k_{\max}} k^p S(k,t)}{\sum_{k=0}^{k_{\max}} S(k,t)} \right)^{1/p}, \tag{3}$$

where $k_{\max}$ is an upper cutoff, we see that a characteristic length can be defined as

$$R^{(1)}(t) = \frac{2\pi}{K_1(t)}. \tag{4}$$

It can be shown that, in isotropic conditions, Wagner's characteristic length $d=d_1=d_2$, can be written in terms of the first and third moments of the structure factor

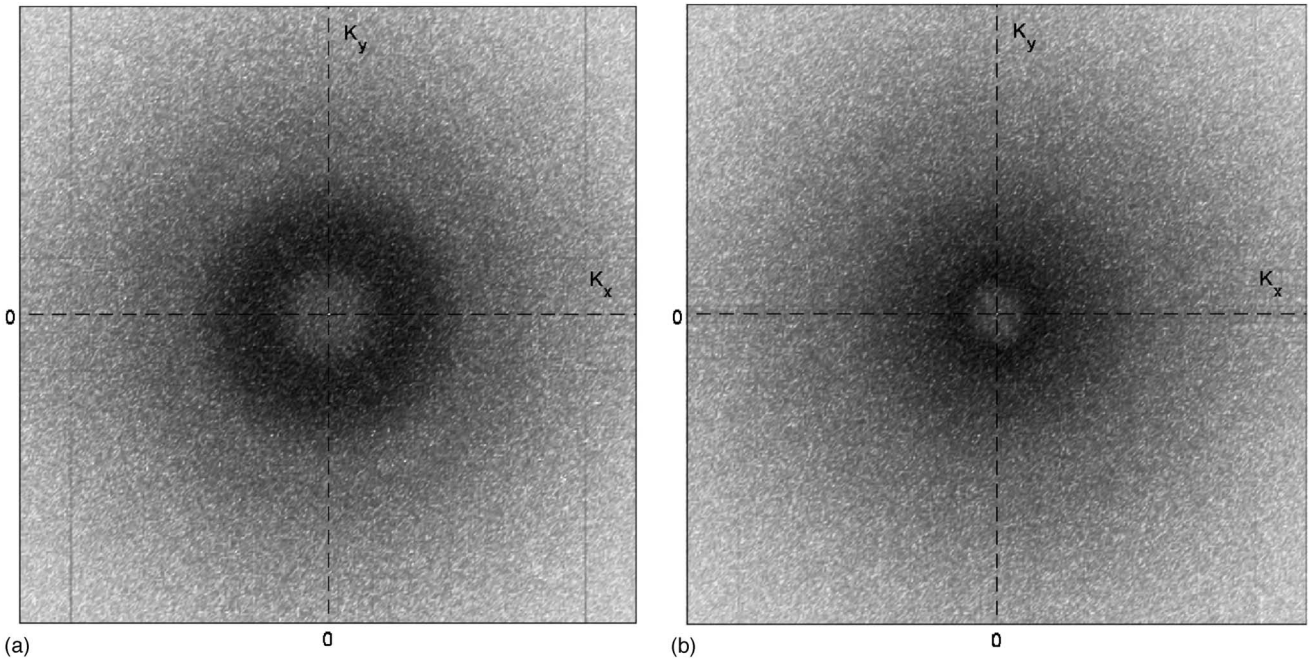


FIG. 6. Fourier transform of two representative snapshots for the critical mixture $\mathcal{A}$ (see Table I).

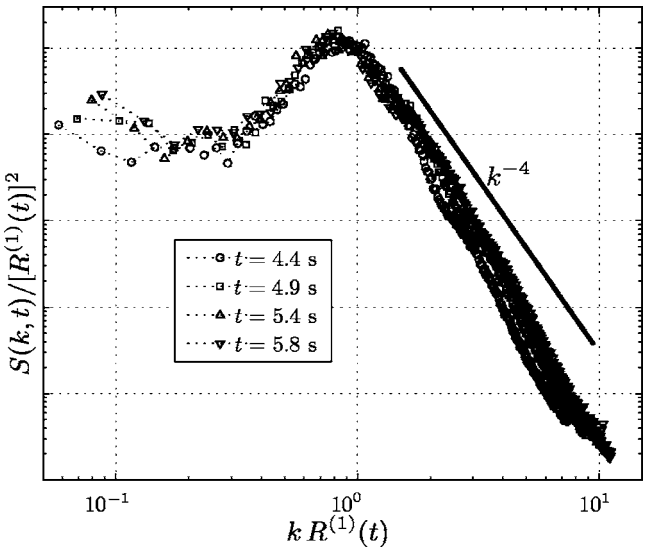


FIG. 7. Dimensionless structure factors as function of dimensionless wavelength at four different times during the convection driven stage for the critical mixture $\mathcal{A}$ (Table I). The continuous line represents the $k^{-4}$ behavior typical of the Porod tail. The quenching rate is $\dot{T}_{\mathrm{lin}}=1.2\ ^{\circ}\mathrm{C/s}$; the critical temperature $T_{\mathrm{cr}}=35\ ^{\circ}\mathrm{C}$ is crossed at $t=3.7$ s.

$$d = 2\pi\frac{K_1}{K_3}. \tag{5}$$

In Fig. 7, the dimensionless structure factor $S(k,t)/[R^{(1)}(t)]^2$ is plotted versus the dimensionless wavelength $kR^{(1)}(t)$ at four different times showing that all plots collapse on a master curve when properly scaled. It should be stressed, however, that this so called structural self-similarity is not enough to guarantee the self-similarity of the structure [14].

The log-log plot of the structure factors reported in Fig. 9 is consistent with analogous results obtained from light-scattering experiments by Guenoun *et al.* [3], who showed that the structure factor obtained by direct visualization carries the same pieces of information as the one obtained from light-scattering experiments. In particular, we see the typical $k^4$ increase for $k<(R^{(1)})^{-1}$ and the expected generalized Porod tail, showing a $1/k^4$ decrease for $k>1/R^{(1)}$.

During the linear, convection-driven stage, the structure factor is single peaked, and therefore double phase transition is not observed, as confirmed also by direct observation. At later stages, however, we notice the appearance of a secondary nucleation structure (Fig. 8), characterized by droplets of one phase within the other (see Table II). Unfortunately, we cannot quantify the evolution of this secondary structure, since when it appears gravity has already begun to influence the process and the primary structure starts sedimenting. Finally, note that, in agreement to Tanaka's experiments [15], we observe double phase separation only in critical mixtures.

The presence of double phase separation rises questions on the hypothesis of local equilibrium [15], as all the coarsening mechanisms that have been proposed to explain the late-stage phase separation are based on the local equilibrium

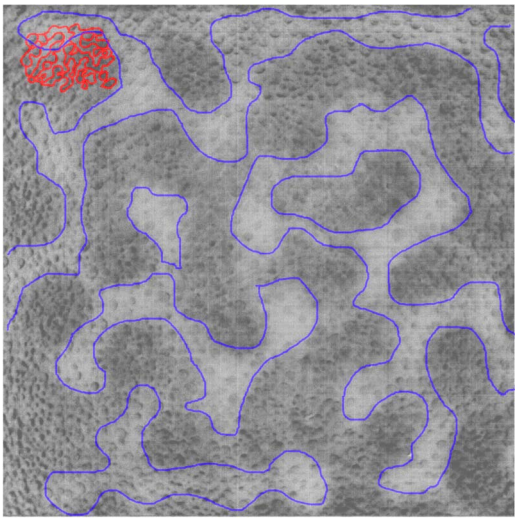

FIG. 8. (Color online) The primary bicontinuous structure is emphasized by hand-drawn interface contours; within the bicontinuous structure, a secondary structure of smaller domains is clearly observed only for critical mixture $\mathcal{A}$ (Table II).

assumption (i.e., the compositions of both phases coincide with their final equilibrium values). Departure from the local-equilibrium assumption may affect their growth rate and even the scaling, and needs to be further investigated. However, as noticed by Tanaka [15], the scaling relation is not so sensitive to a slight deviation of the concentration from the final equilibrium value.

In Fig. 9, the characteristic domain size $R^{(1)}(t)$ is plotted as a function of time. Before the temperature of the mixture reaches the critical point, the characteristic length is almost constant and its value depends on some dust spots present in the field of view. As the temperature of the mixture reaches the critical value ($T=T_{\mathrm{cr}}=35\ ^{\circ}\mathrm{C}$ at time $t=t_{\mathrm{cr}}=3.3$ s), $R^{(1)}$ decreases very rapidly. However, at the start of spinodal decomposition, the actual characteristic length is still small compared to the disturbances and therefore $R^{(1)}$ shows a delay and a decreasing behavior that has been previously reported also in numerical simulations [16]. Eventually, at $t^*\approx 3.6$ s, $R^{(1)}$ begins to capture the actual domain size, and from then on it increases linearly with time, until the sedimentation crossover $L_g$ is reached, and domains start sedimenting, or floating, under the effect of gravity, and the characteristic length $R^{(1)}$ becomes meaningless due to strong anisotropy of the process thereafter.

The characteristic length can be fitted through the linear relation $R^{(1)}(t)=v_{\mathrm{gr}}(t-t^*)$, showing that the process is domi-

TABLE II. Properties of the critical mixture at equilibrium at 15 °C [12].

| | |
|---|---|
| $\Delta\rho$ | $10\ \mathrm{kg/m^3}$ |
| $\mu$ | $10^{-3}\ \mathrm{N\,s/m^2}$ |
| $\sigma$ | $10^{-2}\ \mathrm{N/m}$ |
| $a$ | $10^{-7}\ \mathrm{m}$ |
| $D$ | $5\times10^{-10}\ \mathrm{m^2/s}$ |

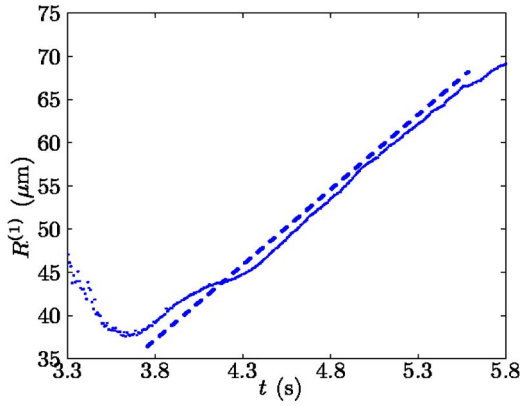


FIG. 9. (Color online) Temporal evolution of the characteristic domain size $R^{(1)}(t)$ [Eq. (4)] for critical mixture $\mathcal{A}$.

nated by convection, with a growth rate that depends on the cooling rate (i.e., the time derivative of the mixture temperature), and not on the temperature itself. The linear growth behavior of $R^{(1)}$ is well documented for shallow quenching (i.e., for $\tau \approx 10^{-5}$), but only limited evidence is available for deep quenching [17]. It is also worth noting that while the linear growth regime is predicted for isothermal phase transitions, in our case we find a similar behavior even though during the process the temperature of the mixture keeps changing. The growth rate depends on the mixture properties as well as the quenching rate, as discussed in Sec. III B. Such delay time $t^* - t_{cr}$ is strongly sensitive to the initial and boundary conditions, as already reported in Ref. [16].

### B. Effect of quenching rate on the growth rate

Thermal history may play an important role on the dynamics of phase separation. In this section, we investigate the influence of the quenching rate on the growth rate during the linear isotropic period of the phase separation. First, we define the quenching rate as

$$\dot{T}_{\mathrm{lin}} = -\frac{1}{t_{\mathrm{end}} - t^*} \int_{t^*}^{t_{\mathrm{end}}} \frac{dT}{dt}(t)dt, \tag{6}$$

where $T$ is the mean temperature measured by the thermocouples inserted in the mixture, while $t^*$ and $t_{\mathrm{end}}$ represent the

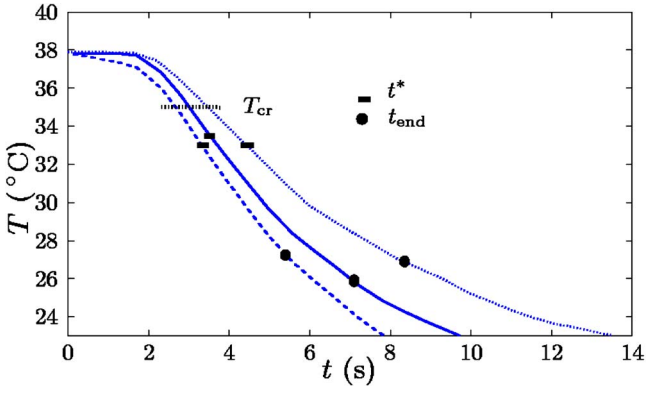


FIG. 10. (Color online) Temperature of the mixture inside the cell as a function of time during the quenching of critical mixture $\mathcal{A}$. The marks on the curves correspond to the beginning and the end of the time interval of linear isotropic growth.

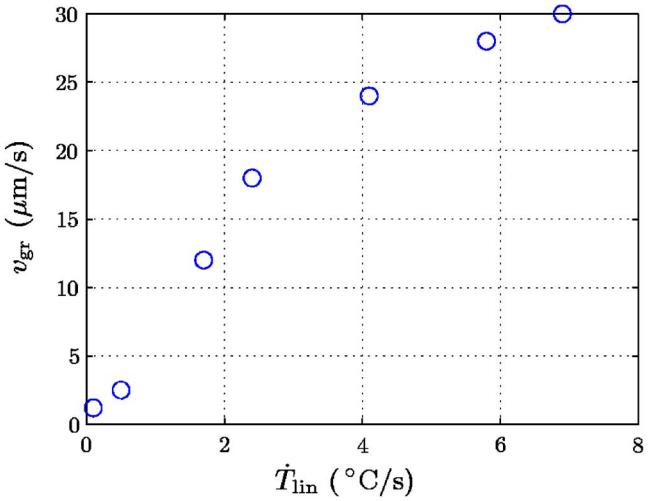


FIG. 11. (Color online) Growth rate as function of the quenching rate.

beginning and the end of the linear isotropic period. In Fig. 10, the temperature of the mixture inside the cell is reported as a function of time for a few experiments, together with the beginning and the end of the linear isotropic period.

In Fig. 11, the growth rate of the single-phase domains $dR^{(1)}/dt$ is shown as a function of the quenching rate $\dot{T}_{\mathrm{lin}}$. It is an increasing function, with a slope at low quenching rates of $O[10\ \mu\mathrm{m\ s^{-1}/(K\ s^{-1})}]$, which is roughly of the same magnitude as that obtained in previous experimental works [12,18].

Figure 11 reveals that increasing the quenching rate, $v_{\mathrm{gr}}$ increases until it reaches an asymptotic value of 37 $\mu$m/s, which corresponds to an instantaneous quenching $\dot{T}_{\mathrm{lin}} \to \infty$. As shown in Table III, as the quenching rate increases, the linear isotropic stage gets shorter, while the size of the domains at the end of this stage increases. From this it appears that the quenching rate can be used to manipulate the separation process and obtain, for instance, domains of the desired size. On the other hand, the separation process can be sped up by increasing the quenching rate, with obvious implications on the design of separation equipment.

In case of instantaneous quenching, applying the diffuse interface model (see Appendix B) we can estimate the do-

TABLE III. Influence of the quenching rate $\dot{T}_{\mathrm{lin}}$ on the growth rate $v_{\mathrm{gr}}$, the duration of the linear growth period $\Delta t = t_{\mathrm{end}} - t^*$, and the domain size at the end of the linear period $L_{\mathrm{end}}$.

| $\dot{T}_{\mathrm{lin}}$ °C/s | $v_{\mathrm{gr}}$ $\mu$m/s | $\Delta t$ s | $L_{\mathrm{end}}$ $\mu$m |
|---|---|---|---|
| 6.9 | 30 | 0.8 | 90 |
| 5.8 | 28 | 0.97 | 81 |
| 4.1 | 24 | 1.2 | 77 |
| 2.4 | 18 | 1.5 | 65 |
| 1.7 | 12 | 2.1 | 55 |
| 0.5 | 2.5 | 3.1 | 40 |
| 0.1 | 1.2 | 3.7 | 36 |

main size growth rate $dL/dt$ starting from the relation

$$\frac{dL}{dt} = 2\frac{J_\phi}{\rho}, \tag{7}$$

which follows [4] both from the mass balance $d(\rho\pi L^3/6)/dt = J_\phi \pi L^2$ valid for spherical domains of diameter $L$ typical of off-critical mixtures, and from the balance $d(\rho\pi L^2/4)/dt = J_\phi \pi L$ valid for dendritic-arm domains of width $L$. Here, $J_\phi$ is the antidiffusive flux that can be approximated as [10]

$$J_\phi \sim \rho D[2\Psi\hat{\phi}(1-\hat{\phi}) - 1]\nabla\phi, \tag{8}$$

where $\hat{\phi}$ is the mean concentration across the interface thickness, $\Psi$ is the Margules parameter (see Appendix B), and $D$ is the molecular diffusivity. We may estimate $\nabla\phi$ as $\Delta\phi/l$, where $l$ is the characteristic interface thickness $l \sim a/\sqrt{\Psi-2}$ [19] and $a$ the van der Waals characteristic length of concentration inhomogeneities, which is related to the surface free energy by the expression (Appendix A) $a \sim 2M_W\chi/3(\Psi-2)^{3/2}\rho RT$. Considering that, near the critical composition, $\Delta\phi \sim \sqrt{3(\Psi-2)/2}$ (Appendix A), we obtain $\nabla\phi \sim \sqrt{3/2}(\Psi-2)/a$. From Eqs. (7) and (8), it follows that the characteristic domain size $L$ grows in time according to the relation

$$\frac{dL}{dt} \sim K\frac{D}{a}, \quad K = \sqrt{3/2}(\Psi-2)[4\Psi\hat{\phi}(1-\hat{\phi}) - 2]. \tag{9}$$

For values of $\hat{\phi}$ around 0.5, we obtain $K \sim \sqrt{3/2}(\Psi-2)^2$, and substituting the expression of $a$ in terms of $\chi$, we may rewrite Eq. (9) in the form

$$\frac{dL}{dt} \sim 12\sqrt{3}\frac{\tau^{7/2}D\rho RT_{cr}}{M_W\chi}, \tag{10}$$

where we consider that, near the critical point $T \sim 2T_{cr}/\Psi$ and $\Psi - 2 \approx 2\tau$, with $\tau = (T_{cr}-T)/T_{cr}$.

The data in Fig. 11 (Table III) are correlated by $v_{gr} \sim \{1-\exp[-\dot{T}_{lin}/(4\ \mathrm{K\ s^{-1}})]\}37\ \mu\mathrm{m/s}$, and hence in the limit of infinite quenching rate the growth rates appear to saturate around 37 $\mu$m/s. Using this asymptotic value for $dL/dt$ in Eq. (10), a value $\chi = \sigma$, and the values of $\rho$, $\sigma$, $D$ from Table II, $M_W = 22.6$ kg/kmol, $T_{cr} = 308$ K (mixture $\mathcal{A}$) we obtain $\Psi = 2.035$. This value yields the estimates $a \sim 0.01$ $\mu$m and $l \sim 0.05$ $\mu$m in good agreement with the orders of magnitude expected on the basis of previous work [10,19]. It also yields $T \sim 2T_{cr}/\Psi = 29.7$ °C, a value in good agreement with the measured temperatures (Fig. 10).

Equation (10) together with our observation that $dL/dt$ remains constant (Fig. 9) even though $T$ changes (Fig. 10) during this segregation regime, indicates that $\chi$ scales as $\tau^{7/2}$ and therefore $a$ scales as $\tau^2$. We conclude from the foregoing estimates that the diffuse interface model captures much of the physics involved and is simple enough to allow to understand the influence of the different parameters.

### C. The effect of viscosity on the growth rate

In this section we report preliminary experimental data on the influence of viscosity on the phase separation of a deeply quenched mixture. To obtain them, we modify the viscosity of the mixture by adding CMC (up to 6% in weight) to $\mathcal{B}$ and $\mathcal{C}$ off-critical mixtures. Now, CMC is soluble with water and immiscible with the organic solvent; in addition, during the phase separation of the $\mathcal{B}$ mixture, the water-rich phase constitutes the discrete, droplike phase, while for the $\mathcal{C}$ mixture it represents the continuous phase. Therefore, when CMC is added to the $\mathcal{B}$ mixture, it increases the viscosity of the continuous phase, while when it is added to the $\mathcal{C}$ mixture, it increases the viscosity of the discrete phase.

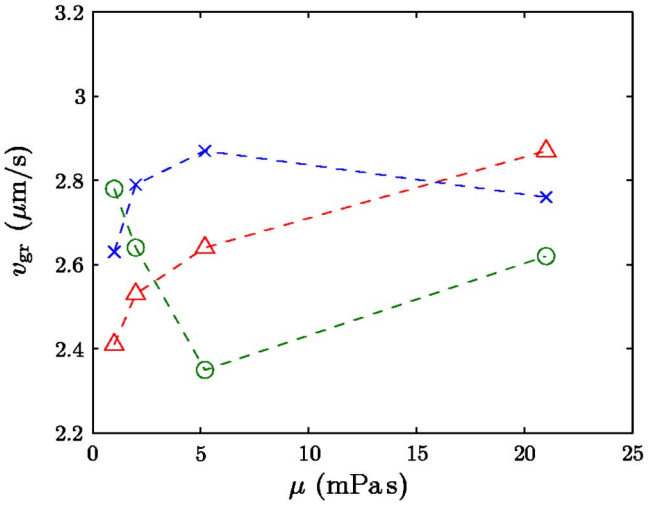


FIG. 12. (Color online) Growth rate as function of the viscosity of the continuous phase; the quenching rate is fixed at 0.5 °C/s. Each symbol represents a set of experimental conditions (same focal plane, same illumination).

Viscosity influences the phase separation process by changing both the growth rate of the domains and their settling velocity. Naturally, viscosity is also important as it contributes to determine the separation regime (diffusion- or convection or diffusion driven): here, however, we assume that the process is always dominated by convection and we look at the effect of viscosity within this regime.

First of all, we measure the isotropy index $\xi$ and see that the process remains isotropic, despite CMC being a long-chained polymer. Then, we check that even at large viscosities the process is indeed still convection driven. Consequently, we always identify a stage where the characteristic length grows as $t$, and we measure the growth rate during that stage.

Figures 12 and 13 indicate that the growth rate does not change significantly when the viscosity of the continuous and discrete phase, respectively, is increased up to 20 times its original (waterlike) value. Furthermore, the self-similarity of the dimensionless structure factor still holds, even for experiments with different viscosity. This is in agreement with the conclusion of Ref. [16], where it is noted that the scaling of the structure factor holds even for slightly different conditions as long as the compared experiments are in the same (convective or diffusion) regime. Therefore, we may conclude that both the growth rate and the general morphology of the mixture result uninfluenced by addition of CMC, regardless of whether it is added to the continuous or to the

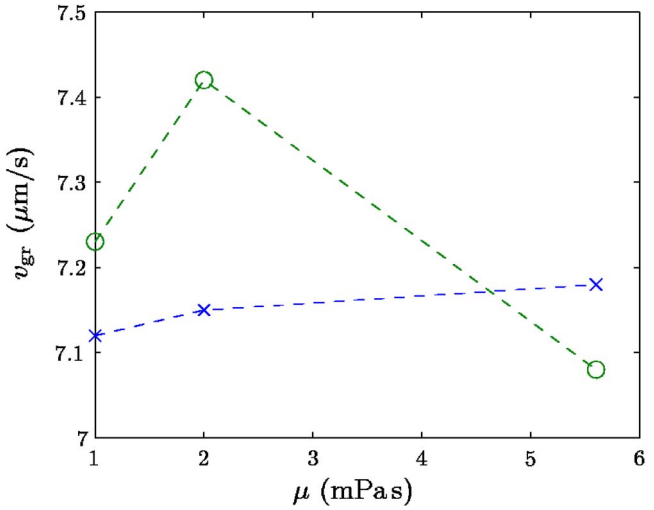


FIG. 13. (Color online) Growth rate as function of the viscosity of the discrete phase; the quenching rate is fixed at 1.2 °C/s. Each symbol represents a set of experimental conditions (same focal plane, same illumination).

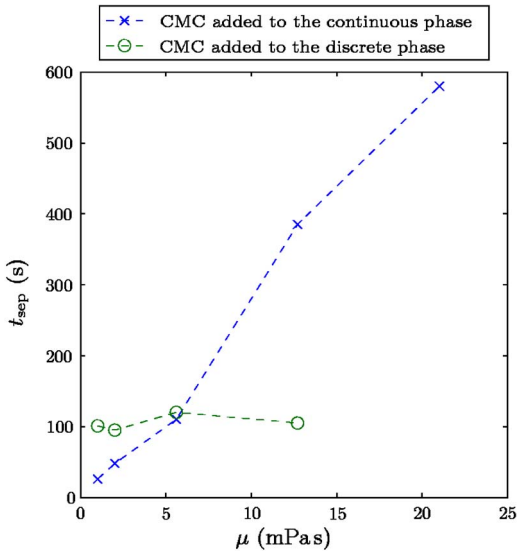


FIG. 14. (Color online) Separation time $t_{sep}$ by gravity as function of the viscosity $\mu$ of the continuous phase (×) and the discrete phase (○).

discrete phase. Thus, by changing the viscosity we cannot control the separation rate during the convection-driven stage before the gravitational crossover.

The independence of the growth rate on viscosity is in agreement with the prediction of the diffuse interface model [20], since Eq. (10) shows that $dL/dt$ is independent of viscosity. However, this model is based on the hypothesis that the two components of the mixture have the same viscosity, which contrasts with our experimental conditions. In addition, when adding CMC to water, other properties, such as mass diffusivity, may also change. Therefore, it is remarkable that, despite all that, the diffuse interface model seems able to predict, at least qualitatively, the behavior of the mixture as it phase separates.

After the gravitational crossover, instead, as expected, viscosity does influence the settling speed and, hence, the separation time. In fact, it is well known that the sedimentation velocity of a single droplet in an unbounded fluid is inversely proportional to the viscosity of the continuous phase through the Hadamard-Rybczynski equation [21]. Accordingly, we measured the separation time for different values of the viscosity of the continuous and of discrete phase, where by separation time we denote the time needed to form a sharp and stable interface. Results are presented in Fig. 14. As expected, increasing the viscosity of the continuous phase, a linear increase of the separation time is observed, as the droplet settling velocity decreases, so that the separation increases proportionally. On the contrary, changing the viscosity of the discrete phase only, has no effects on the sedimentation time.

## IV. DISCUSSION AND CONCLUSION

In this paper, we discuss and analyze a set of new experimental results on the deep quenching of liquid binary mixtures. We show that after a diffusion and viscosity controlled initial delay, a convection driven stage follows, in which domains grow linearly with time up to when gravitational effects take over. We also find structure factors that are self-similar and, at large wavelength, approach the Porod tail.

When the mixture is deeply quenched, the quenching time is often (at least in industrial-size equipment) comparable with the characteristic separation time and, hence, quenching cannot be assumed as instantaneous. By investigating the effect of the quenching rate on the growth rate, we find that the growth rate increases with increasing quenching rate, until it approaches an asymptotic value, corresponding to instantaneous quenching. In addition, although the convective stage of the process gets shorter when the quenching rate increases, the size of the single phase domains at the end of this stage appears to increase. These effects may play an important role in industrial applications, and call for an extension of the theoretical models in order to account for the temperature history and cooling rate.

We also investigate the influence of viscosity on phase separation. We find that, in agreement with the predictions of the diffuse interface model, the growth rate of the single-phase domains during the convective stage of phase separation does not depend on the viscosity, regardless of whether we increase the viscosity of the continuous or of the discrete phase. On the other hand, when gravitational effects become relevant, the viscosity of the continuous phase is proportional to the settling time, in agreement with well established theory. These results are quite important because solvents often have a low viscosity at the beginning of the process, but then evolve (e.g., during polymerization processes) into very viscous products.

We find that even when the quench is not instantaneous, there is still a linear growth period as predicted by the *H* model. It is also remarkable that as the cooling rate increases the growth rate approaches the theoretical value. We are not aware of any investigation about the influence of the cooling rate on the linear growth period; in particular the results presented here are obtained for deeply quenched mixtures

for which a detailed experimental characterization is still missing.

The possibility to influence the growth rate has implications in many industrial problems as it can be used to produce domains with the desired size. In particular, viscosity modifiers cannot be used effectively to change the separation time as long as the process is in the convection regime.

## APPENDIX A: THE GENERALIZED FREE ENERGY OF BINARY MIXTURES

Let us consider a homogeneous (uniform) mixture of two species $A$ and $B$ with molar fraction $y_A$ and $y_B$, respectively, temperature $T$ and pressure $p$. The equilibrium state is such that it minimizes the Gibbs molar energy of mixing $\Delta g_0$ defined as

$$\Delta g_0 = g_0 - (g_A y_A + g_B y_B), \tag{A1}$$

where $g_0$ denotes the free energy of the uniform mixture at equilibrium, while $g_A$ and $g_B$ are the energies of the pure species $A$ and $B$ at temperature $T$ and pressure $p$, and subscript 0 indicates that the mixture is uniform. $\Delta g_0$ can be seen as the sum of an ideal part ($\Delta g^{\mathrm{id}}$) and an excess part ($g^{\mathrm{ex}}$). The ideal part can be easily derived by molecular theory [22], obtaining

$$\Delta g^{\mathrm{id}} = RT(y_A \ln y_A + y_B \ln y_B), \tag{A2}$$

where $R$ is the gas constant. The excess part needs to be modeled and, for symmetric mixtures, can be expressed through the one-parameter Margules expression [23]

$$g^{\mathrm{ex}} = RT\Psi y_A y_B, \tag{A3}$$

where $\Psi$ is the dimensionless Margules coefficient (function of $T$ and $p$). In conclusion, denoting by $y_A = \phi$ and $y_B = 1 - \phi$ the molar fractions of the two species, Eq. (A1) becomes (Fig. 15):

$$\Delta g_0 = RT[\phi \ln \phi + (1-\phi)\ln(1-\phi)] + RT\Psi\phi(1-\phi). \tag{A4}$$

It can be easily seen that when $\Psi > 2$, the condition of instability $\partial^2 \Delta g_0 / \partial \phi^2 < 0$ is satisfied in a certain range of composition and the mixture phase separates. The compositions $\phi_1$ and $\phi_2$ of the two coexisting phases at equilibrium across (but far from) a flat interface can be easily determined as a function of $\Psi$ by minimizing the free energy, i.e., from $\partial \Delta g_0 / \partial \phi = 0$. Measuring the composition of the two coexisting phases at different temperatures, one can easily plot the coexistence $\phi - T$ curve, and from that determine the Margules parameter $\Psi$ as a function of temperature $T$ (at constant pressure). For nearly regular mixtures, in the neighborhood of the critical composition ($\phi_{\mathrm{cr}} \sim 0.5$), we may use the leading order approximations $\Delta\phi_{\mathrm{eq},0} = \phi_1 - \phi_2 = \sqrt{3/2}\sqrt{\Psi - 2}$ and $\Psi = 2T_{\mathrm{cr}}/T$.

Now, Eq. (A4) refers to stable equilibrium states in which the composition of the mixture is uniform. To take into account the effects of spatial inhomogeneities, such as within the interfacial region between two phases, following van der Waals' ideas [11], Cahn and Hillard [24] defined the generalized free energy $\tilde{g}$

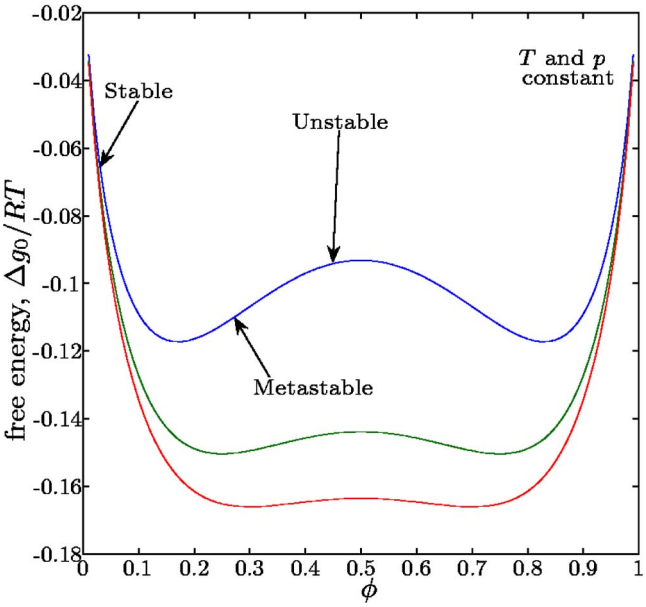


FIG. 15. (Color online) Gibbs free energy of binary mixtures as a function of the composition.

$$\tilde{g} = g_0 - \frac{1}{2}RTa^2(\nabla y_A)(\nabla y_B) = g_0 + \frac{1}{2}RTa^2(\nabla\phi)^2, \tag{A5}$$

where $a$ represents the typical length of spatial inhomogeneities. At equilibrium, and in the neighborhood of the critical composition, this characteristic length can be estimated from surface tension $\sigma$ measurements on flat interfaces [9,12,17]. In fact, denoting by $\chi$ the extra free energy stored in the unit interfacial area, following van der Waals [11] we obtain

$$\chi \sim \frac{\rho RT}{M_W} a^2 \int (\nabla\phi)^2 \hat{\mathbf{n}} \cdot d\mathbf{r}, \tag{A6}$$

where $\hat{\mathbf{n}}$ is the unit vector, normal to the interface, with $\chi = \sigma$ at equilibrium. As a result, we obtain the estimate

$$\chi \sim \frac{3}{2}(\Psi - 2)^{3/2}\frac{\rho RTa}{M_W}, \tag{A7}$$

where we take $\int (\nabla\phi)^2 dr \sim (\Delta\phi_{\mathrm{eq},0})^2 / l$.

With $\Psi \approx 2.035$ and the same data used to estimate Eq. (10) we obtain $a \approx 0.01$ $\mu$m.

## APPENDIX B: THE GOVERNING EQUATIONS OF MOTIONS FOR BINARY MIXTURES

The motion of an incompressible binary mixture composed of two species A and B is described through the so-called $H$ model [5], also known as diffuse interface model [6,7]. The species $A$ and $B$ are assumed to have the same density ($\rho$), viscosity ($\mu$), and molecular weight ($M_W$). Denoting by $\phi$ the molar fraction of $A$, when inertia effects are negligible, conservation of mass and momentum lead to the following equations:

$$\nabla \cdot \mathbf{v} = 0 \tag{B1}$$

$$\frac{\partial \phi}{\partial t} + \mathbf{v} \cdot \nabla \phi = -\nabla \cdot \mathbf{J}_\phi \tag{B2}$$

$$\mu \nabla^2 \mathbf{v} - \nabla p = \mathbf{F}_\phi, \tag{B3}$$

where $\mu$ is the fluid viscosity, $\mathbf{v}$ is the averaged local fluid velocity (or baricentric velocity [25]), $\mathbf{J}_\phi$ is the antidiffusion flux, and $\mathbf{F}_\phi$ is a (nonequilibrium) capillary body force. Equations (B1) and (B2) can be derived from the conservation of species together with the incompressibility condition, while the antidiffusion flux $\mathbf{J}_\phi$ can be determined through a constitutive equation based on irreversible thermodynamics [20]

$$\mathbf{J}_\phi = -\phi(1-\phi) D \nabla \tilde{\pi}, \tag{B4}$$

where $D$ is the molecular diffusivity, while $\tilde{\pi} = \pi_A - \pi_B = \delta \tilde{g} / \delta \phi$ represents the non-dimensional generalized chemical potential difference. Obviously, once the generalized free energy is known [see Eq. (A5)], $\tilde{\pi}$ can be easily determined.

Equation (B3), expressing the conservation of momentum, has been derived mainly heuristically, although a more rigorous derivation has been proposed by Antanovskii [26] through entropy production maximization. Here, $\mathbf{F}_\phi$ is a reversible body force that tends to minimize the energy stored at the interface and, in fact, it represents the divergence of the so-called Korteweg stresses [27],

$$\mathbf{F}_\phi = -\frac{\rho R T}{M_W} \phi \nabla \tilde{\pi}. \tag{B5}$$

This nondissipative nonequilibrium force tends to drive the fluid particles towards the direction in which the chemical potential difference is decreasing, thus driving $A$-rich lumps towards $A$-rich regions and therefore enhancing coalescence among droplets.

Let us consider a mixture composed of single phase domains of uniform, equilibrium concentration, separated by sharp interfaces. At equilibrium, the integral of $\mathbf{F}_\phi$ across an interface must be equal to the surface force $\mathbf{F}_A = \hat{\mathbf{n}} \Delta p$, where $\Delta p$ is the pressure jump across the interface, which is related to the surface tension $\sigma$ by Laplace's law $\Delta p = \sigma \kappa$, where $\kappa$ is the curvature, which for spherical domains of diameter $L$ is $4/L$ and for dendritic-arm domains $2/L$ (this is the case of a critical mixture). So, not only at equilibrium, we have

$$\int \mathbf{F}_\phi \hat{\mathbf{n}} \cdot d\mathbf{r} = \hat{\mathbf{n}} \sigma \kappa. \tag{B6}$$

From this equation, as shown by Pismen [28], we obtain again the relation (A7) between $\chi$ and $a$ (with $\chi = \sigma$ at equilibrium), but we also obtain the estimate $F_\phi \sim 2\chi / lL$, being $l \sim a/\sqrt{\Psi - 2}$ the typical thickness of the interface.

Now, the importance of convection relative to diffusion is controlled by the Péclet number defined as the ratio between convective and diffusive mass fluxes $\mathrm{Pe} = VL/D$, where $L$ is the size of the single-phase domains, while $V$ is a characteristic velocity, which can be estimated from Eq. (B3) as $V \sim F_\phi a^2 / \mu$. Combining this with $F_\phi \sim 2\sigma / lL$ we obtain the following estimate for the convective velocity:

$$V \sim \frac{\chi}{\mu} \frac{2a\sqrt{\Psi - 2}}{L}, \tag{B7}$$

which for our typical values, $\Psi = 2.035$, $a \sim 0.01$ $\mu$m, and $L \sim 35$ $\mu$m, yields $V \sim 1.1$mm/s, which is the order of magnitude of our observed velocities.

For the Péclet number, using Eq. (B7) we obtain

$$\mathrm{Pe} = \frac{VL}{D} \approx 2\sqrt{\Psi - 2} \frac{\chi a}{\mu D} \approx 2\sqrt{2\tau} \frac{\chi a}{\mu D}, \tag{B8}$$

which leads to $\mathrm{Pe} \sim 75$ for the data just cited.

It should be pointed out that in most previous work, another Péclet number $\mathrm{Pe}_a = V' a / D = \sigma a / \mu D$ (based on another typical velocity $V' \sim \sigma / \mu$) has been considered, which derives naturally from the non-dimensionalization of the governing equations. The two definitions yield similar values for $\chi = \sigma$ except for the $2\sqrt{\Psi - 2} \approx 2\sqrt{2\tau}$ factor which in our case ranges between 0.23 and 0.46 (as $\tau$, during the linear growth interval, ranges from 0.006 to 0.026), while during the temperature change from 33 to 27 °C of the linear growth interval (Figs. 9 and 10) the Péclet number Pe ranges between 1.7 and 7600, while $\mathrm{Pe}_a$ between 7 and 16 700. Now, using Eqs. (A7) into (B8) and the result in Eq. (10), we further obtain the relations

$$\mathrm{Pe} \approx \frac{12 \rho R T_{\mathrm{cr}} \tau^2 a^2}{\mu D M_W} \approx \frac{2 M_W \sigma^2}{3 \mu D \rho R T_{\mathrm{cr}} \tau} \approx \frac{288 \rho R T_{\mathrm{cr}} D \tau^6}{\mu M_W (dL/dt)^2}. \tag{B9}$$


[1] Y. C. Chou and W. I. Goldburg, Phys. Rev. A **20**, 2105 (1979).
[2] N.C. Wong and C. M. Knobler, Phys. Rev. A **24**, 3205 (1981).
[3] P. Guenoun, R. Gastaud, F. Perrot, and D. Beysens, Phys. Rev. A **36**, 4876 (1987).
[4] E. D. Siggia, Phys. Rev. A **20**, 595 (1979).
[5] P. C. Hohenberg and B. I. Halperin, Rev. Mod. Phys. **49**, 435 (1977).
[6] D. M. Anderson, G. B. McFadden, and A. A. Wheeler, Annu. Rev. Fluid Mech. **30**, 139 (1998).
[7] J. Lowengrub and L. Truskinovsky, Proc. R. Soc. London, Ser. A **454**, 2617 (1998).
[8] D. Jacqmin, J. Fluid Mech. **402**, 57 (2000).
[9] G. Santonicola, R. Mauri, and R. Shinnar, Ind. Eng. Chem. Res. **40**, 2004 (2001).
[10] N. Vladimirova, A. Malagoli, and R. Mauri, Phys. Rev. E **60**, 2037 (1999).
[11] J. D. van der Waals, J. Stat. Phys. **20**, 200 (1979).
[12] R. Gupta, R. Mauri, and R. Shinnar, Ind. Eng. Chem. Res. **38**, 2418 (1999).
[13] R. Gupta, R. Mauri, and R. Shinnar, Ind. Eng. Chem. Res. **35**, 2360 (1996).
[14] A. Wagner, Ph.D. thesis, University of Oxford, 1997.

[15] H. Tanaka, Phys. Rev. E **51**, 1313 (1995).
[16] V. M. Kendon, M. E. Cates, I. Pagonabarraga, J. C. Desplat, and P. Bladon, J. Fluid Mech. **440**, 147 (2001).
[17] R. Mauri, F. Califano, E. Calvi, R. Gupta, and R. Shinnar, J. Chem. Phys. **118**, 8841 (2003).
[18] F. Califano and R. Mauri, Ind. Eng. Chem. Res. **43**, 349 (2004).
[19] R. Mauri, R. Shinnar, and G. Triantafyllou, Phys. Rev. E **53**, 2613 (1996).
[20] N. Vladimirova, A. Malagoli, and R. Mauri, Chem. Eng. Sci. **55**, 6109 (2000).
[21] W. M. Deen, *Analysis of Transport Phenomena* (Oxford University Press, Oxford, 1998), p. 326.
[22] J. M. Prausnitz, R. N. Lichtenthaler, and E. Gomes de Azevedo, *Molecular Thermodynamics of Liquid Phase Equilibria* (Prentice-Hall, New York, 1986).
[23] E. P. Gyftopolous and G. P. Beretta, *Thermodynamics: Foundations and Applications* (Dover Publications, Mineola, NY, 2005).
[24] J. W. Cahn and J. E. Hilliard, J. Chem. Phys. **31**, 688 (1959).
[25] S. R. DeGroot and P. Mazur, *Non Equilibrium Thermodynamics* (Dover Publications, Mineola, NY, 1962).
[26] L. K. Antanovskii, Phys. Rev. E **54**, 6285 (1996).
[27] L. M. Pismen and Y. Pomeau, Phys. Rev. E **62**, 2480 (2000).
[28] L. M. Pismen, Phys. Rev. E **64**, 021603 (2001).